Separation of intra- and intergranular magnetotransport properties in nanocrystalline diamond films on the metallic side of the metal–insulator transition

2011 New J. Phys. 13 083008

(http://iopscience.iop.org/1367-2630/13/8/083008)

New Journal of Physics
The open-access journal for physics

Separation of intra- and intergranular magnetotransport properties in nanocrystalline diamond films on the metallic side of the metal–insulator transition

S D Janssens[1,6], P Pobedinskas[1], J Vacik[2], V Petráková[3,4], B Ruttens[1,5], J D'Haen[1,5], M Nesládek[1,5], K Haenen[1,5,6] and P Wagner[1,5]

[1] Institute for Materials Research (IMO), Hasselt University, Wetenschapspark 1, 3590 Diepenbeek, Belgium
[2] Nuclear Physics Institute, Academic Science CR, v.v.i., and Research Center Rez, 25068 Husinec - Rez, Czech Republic
[3] Institute of Physics, Academic Science CR, v.v.i., Cukrovarnicka 10, 16253 Prague 6, Czech Republic
[4] Faculty of Biomedical Engineering, Czech Technical University, Prague, Sitna sq. 3105, 272 01 Kladno 2, Czech Republic
[5] IMOMEC, IMEC vzw, Wetenschapspark 1, 3590 Diepenbeek, Belgium
E-mail: sdjansse@gmail.com and ken.haenen@uhasselt.be

New Journal of Physics **13** (2011) 083008 (18pp)
Received 6 March 2011
Published 9 August 2011
Online at http://www.njp.org/
doi:10.1088/1367-2630/13/8/083008

Abstract. A systematic study on the morphology and electronic properties of thin heavily boron-doped nanocrystalline diamond (NCD) films is presented. The films have nominally the same thickness (≈150 nm) and are grown with a fixed B/C ratio (5000 ppm) but with different C/H ratios (0.5–5%) in the gas phase. The morphology of the films is investigated by x-ray diffraction and atomic force microscopy measurements, which confirm that lower C/H ratios lead to a larger average grain size. Magnetotransport measurements reveal a decrease in resistivity and a large increase in mobility, approaching the values obtained for single-crystal diamond as the average grain size of the films increases. In all films, the temperature dependence of resistivity decreases with larger grains and the charge carrier density and mobility are thermally activated. It is possible

[6] Authors to whom any correspondence should be addressed.

to separate the intra- and intergrain contributions for resistivity and mobility, which indicates that in these complex systems Matthiessen's rule is followed. The concentration of active charge carriers is reduced when the boron-doped NCD is grown with a lower C/H ratio. This is due to lower boron incorporation, which is confirmed by neutron depth profiling.

Contents

1. Introduction

Nanocrystalline diamond (NCD) thin films are known for their outstanding properties such as high hardness, high Young's modulus, high thermal conductivity, rich electronic transport behavior, excellent biocompatibility and more. Therefore, a variety of applications has been reported such as tunable optical lenses [1], high-frequency (surface) acoustic (wave) devices [2, 3], microelectromechanical systems (MEMS) [4], metal-semiconductor field-effect transistors (MESFETs) [5], solar cells [6] and bioelectrochemical applications [7–10].

Studies performed on NCD [11–20] show that the main parameters to grow different types of NCD are temperature, pressure, amount and type of doping, C/H ratio in the gas phase (ξ), substrate, substrate pretreatment, type of chemical vapor deposition (CVD) reactor and power density. For microcrystalline diamond or NCD, temperature, pressure, power density and C/H ratio in the gas phase lead to different growth rates, sp^2/sp^3 carbon ratios, grain sizes and crystal orientations [21–23]. Boron doping of NCD leads to a wide range of electronic transport properties with a critical boron concentration for the metal–insulator transition between 2×10^{20} and 3×10^{20} cm^3 [24, 25]. For boron concentrations higher than 10^{21} cm^3, NCD can be superconducting below liquid helium temperatures [26, 27].

In this work, the influence of the C/H ratio on the transport properties of boron-doped NCD (B:NCD) above the metal–insulator transition [28, 29, 30], grown by microwave plasma-enhanced chemical vapor deposition (MPECVD), is investigated. The samples have boron concentrations ranging from 3.3×10^{21} to 5.3×10^{21} cm^{-3}, although similar amounts of doping gas are used during deposition. To compare the morphology, structure and electronic properties, x-ray diffraction (XRD), atomic force microscopy (AFM), optical reflection spectroscopy in the ultraviolet-to-visible (UV-VIS) light region, neutron depth profiling (NDP), Hall effect and resistivity measurements are performed.

It is shown that samples grown with a lower C/H ratio have a larger average grain size, a lower resistivity (ρ), a higher hole mobility (μ), a less pronounced resistivity drop with increasing temperature, less boron incorporation, which was already suggested for single-crystal

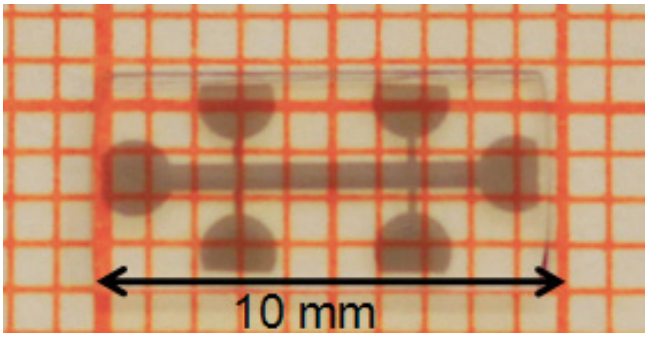

Figure 1. A 10 mm × 5 mm Hall bar pattern of 150 nm thick B:NCD on fused silica. The width of the conduction path is 0.6 mm and the width of the paths to the contacts for the voltage measurements is 0.2 mm.

diamond [31], and fewer active charge carriers. All samples also show a slight increase in hole mobility and hole density with increasing temperature.

2. Experimental

Diamond growth was carried out in an ASTeX 6500 series MPECVD reactor on an electrically isolating fused silica substrate that was treated with a colloidal suspension of 5–10 nm detonation diamond [32]. The temperature was monitored by a Williamson Pro92 dual-wavelength pyrometer. Growth was performed in a CH_4/H_2 plasma with methane concentrations up to 5%. Doping was induced by trimethyl boron gas ($B(CH_3)_3$) with a 5000 ppm B/C ratio for all samples. The substrate temperature was 700 °C induced by 3500 W of microwave power at a total pressure of 33 hPa (25 torr). The growth was stopped when the B:NCD layers reached a thickness of ≈150 nm and cooling down was done under hydrogen flow. The thickness was determined *ex situ*, at standard ambient conditions, from interference fringes of a UV-VIS reflection spectrum. In total, nine samples were made by linearly decreasing the C/H ratios from 5 to 0.5% in steps of 0.5%, generating a set of samples with grains increasing in size due to the decrease in the C/H ratio. An examination of the surface morphology was performed with an atomic force microscope (NTEGRA Prima NT MDT) under tapping mode and at standard ambient conditions. The XRD study for the (111) crystal plane was carried out with a Siemens D5000 θ–2θ Bragg–Brentano diffractometer using the Cu $K_{\alpha 1}$ line (0.15406 nm). In order to perform electronic transport measurements, the samples were etched into a Hall bar pattern (figure 1) using an oxygen plasma (3 min, 300 W, 5.6×10^{-3} hPa) in combination with a protective Al mask (200 nm) produced by magnetron sputtering and lift-off photolithography. This procedure allows complete removal of the unmasked B:NCD parts, exposing the fused silica substrate. After removing the Al mask with an etchant, six circular Ti/Al contacts (50 nm/200 nm) with a diameter of 1.5 mm were deposited by magnetron sputtering [33]. Resistivity and Hall effect measurements were performed in an Oxford instruments MicrostatHe cryostat. The Hall effect was measured with a tapered pole electromagnet (Bruker) by alternating a 2 T magnetic field, reaching a complete reversal of the field in less than 20 s. The total boron concentration, with an error of 10%, was determined with NDP at standard ambient conditions [34–36].

Table 1. Summary of the morphological characteristics of B:NCD films as a function of C/H ratio during the growth of diamond films. Grain size (d) and log-normal grain size distribution (σ) are calculated from XRD spectra, and RMS (surface) roughness is calculated from AFM measurements.

C/H ratio (%)	Growth rate (nm min^{-1})	d (nm)	σ	RMS roughness (nm)
0.5	1.2	–	–	–
1	2.0	67 ± 3	0.70 ± 0.04	18.4
1.5	2.8	76 ± 4	0.72 ± 0.05	–
2	3.5	61 ± 3	0.67 ± 0.06	15.3
2.5	3.8	59 ± 2	0.66 ± 0.06	–
3	4.4	50 ± 2	0.66 ± 0.06	13.2
3.5	4.6	55 ± 2	0.71 ± 0.05	–
4	4.9	54 ± 2	0.67 ± 0.06	12.0
4.5	5.0	52 ± 2	0.70 ± 0.04	–
5	5.1	47 ± 2	0.7 ± 0.05	8.2

3. Results and discussion

3.1. Structural properties

The average grain size for thin NCD layers depends on the thickness of the layers and on the C/H ratio when all the other growth parameters are kept constant. Therefore, all samples were grown to a fixed thickness of 150 ± 15 nm confirmed by UV-VIS reflection interferometry. The growth rates, listed in table 1, decrease with decreasing C/H ratio. Figure 2 shows increasing grain size with decreasing C/H ratio together with root mean square (RMS) surface roughness, calculated from the AFM measurements, which is also listed in table 1. This correlates nicely with the increase in grain size as the C/H ratio decreases. After XRD experiments, the Scherrer equation was used to calculate the mean size (τ) of the crystalline domains in the films [37]:

$$\tau = \frac{K\lambda}{\beta \cos\theta} \leqslant d, \tag{1}$$

where K is the shape factor, λ is the x-ray wavelength, β is the line broadening at half the maximum intensity (full-width at half-maximum (FWHM)) in radians, θ is the Bragg angle and d is the grain size. This method is used to measure through the complete film and is complementary to AFM, which is used to measure the surface size of the grains. It is hard to define the shape factor for NCD films since the grains of polycrystalline diamond are known to grow as inverted pyramids [38], i.e. with larger but fewer grains when approaching the surface. Nevertheless, in many cases a value of 0.9 is a good approximation [39]. To estimate the FWHM for solving the Scherrer equation, a pseudo-Voigt function fit [40] is used and instrumental broadening is taken into account. The error on the grain size is derived with error propagation from the error on the FWHM. The grain size distribution (σ) and its error are derived from a model proposed by Sánchez-Bajo *et al* [41]. In this model, σ is assumed to be log-normal and calculated with the mixing parameter of the pseudo-Voigt function fit. The most intense (111) crystal plane is used since there is almost no preferential crystal orientation for thin NCD layers.

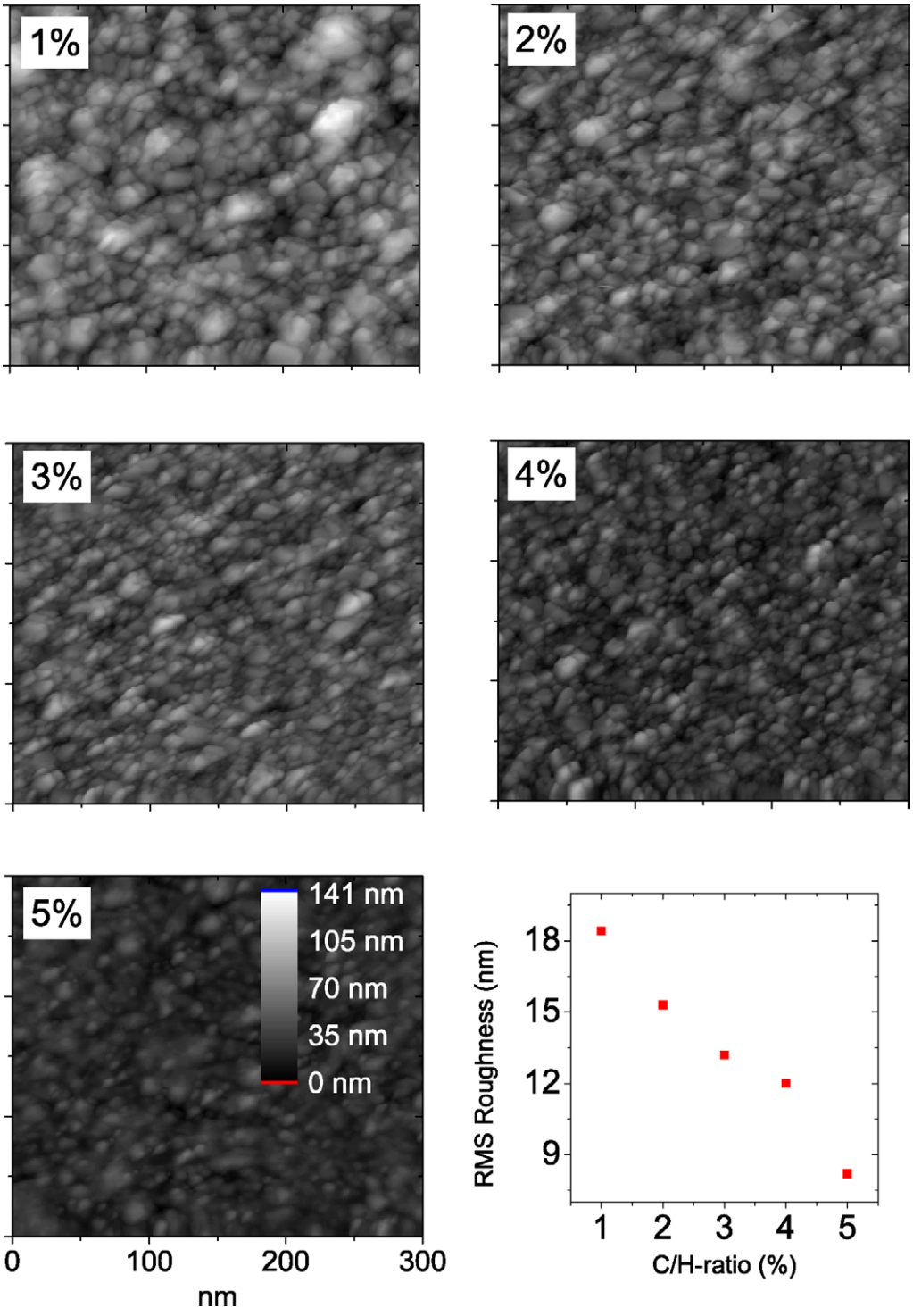

Figure 2. AFM images of the 1–5% samples. The images are identically scaled, which visualizes the decrease in grain size and the decrease in surface roughness as a function of C/H ratio. Scale bars are shown on the image of the 5% sample. Additionally, RMS (surface) roughness is plotted as a function of C/H ratio.

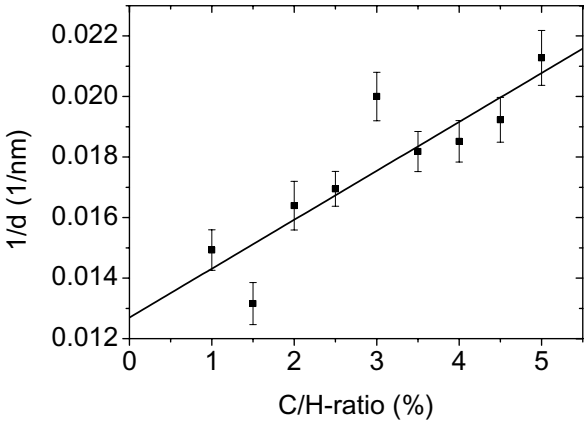

Figure 3. Relation between the average grain size of the thin B:NCD layers derived from XRD measurements and the C/H ratio during the growth of the layers.

With decreasing C/H ratio, the grains are estimated to be ≈50 to ≈70 nm in diameter (table 1) on neglecting possible strain in the layers, which can give additional broadening and a subsequent underestimation of grain size. In the literature, AFM and scanning tunneling microscopy (STM) measurements on thin B:NCD layers [25, 42] give a grain size about twice the value of the XRD values obtained here. This is an acceptable difference since the largest part of the inverse pyramid (grain) is present at the surface. The grain size distribution (σ), on the other hand, shows no significant trend as a function of C/H ratio (table 1).

A combination of modeling and experimental data gives a formula that describes the influence of the C/H ratio on the maximum grain size in nm [18]:

$$d = \{2.25 + 0.67\mathrm{e}^{3430/T_s}\}\{[\mathrm{H}]/[\Sigma \mathrm{CH}_x]\}, \tag{2}$$

where T_s is the substrate temperature in kelvin, [H] the concentration of atomic hydrogen and $[\Sigma \mathrm{CH}_x]$ the concentration of hydrocarbon radicals ($x < 4$) in the plasma. One can assume that [H] is constant compared to $[\Sigma \mathrm{CH}_x]$ for all C/H ratios used in this work. Since the plasma during the CVD has an abundance of hydrogen which reacts with methane, $[\Sigma \mathrm{CH}_x]$ decreases linearly on decreasing the C/H ratio linearly. Also, assuming that the latter equation is qualitatively usable for thin NCD films, where the grains are not yet fully grown, equation (2) can be written as

$$\frac{1}{d} = A_d \xi + B_d = A_d \xi + \frac{1}{d_0}. \tag{3}$$

In figure 3, using the grain sizes derived from XRD spectra, a trend that supports the latter equation is seen, with A_d the slope and B_d the intercept of a least-squares linear fit. The quantity d_0 represents the average grain size at a theoretical C/H ratio of 0%. It has already been shown that lower C/H ratios lead to larger grains. For the asymptotic case of an extremely low C/H ratio in combination with an extremely long growth time, this would lead to a very large grain, i.e. a quasi-mono crystal. However, in figure 3, data from films of 150 nm are presented, i.e. are very limited in deposition time. This leads to a nonzero intercept with the y-axis. The d_0 value (≈80 nm) derived in figure 3 is expected to be of the order of the thickness of the investigated films (150 nm). As mentioned above, strains can lead to additional broadening, which leads

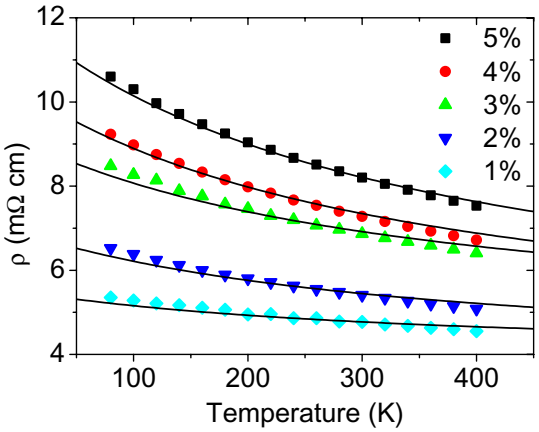

Figure 4. Resistivity as a function of temperature for different C/H ratios. The black lines represent the fittings using equation (6) with ρ_0 as the only fitting parameter.

to an underestimation of the grain size and for grains with a size above 100 nm, the Scherrer equation is not valid.

3.2. Electronic properties

In heavily boron-doped single-crystal diamond and large-grained microcrystalline diamond, the change in resistivity with temperature ($\partial\rho/\partial T$) is small and positive on the metallic side of the metal–insulator transition [24, 28, 43, 44]. This is a trend also observed in other doped single-crystal/polycrystalline semiconductors. In general, in polycrystalline semiconductors, grain boundaries can be represented as a potential barrier for charge carriers, which makes $\partial\rho/\partial T$ negative due to thermal activation [25, 45]. This means that more charge carriers will pass the grain boundaries as they gain energy with the increasing temperature and that the mobility increases as a function of temperature ($\partial\mu/\partial T > 0$). For the sake of completeness, it must be mentioned that a charge carrier density increase and ionized impurity scattering (at elevated temperatures) can also make $\partial\rho/\partial T$ negative [46]. Taking into account the properties of grain boundaries, one can imagine that a grain boundary density increase leads to a higher resistivity, a lower mobility, a more negative $\partial\rho/\partial T$ and a more positive $\partial\mu/\partial T$.

Although heavily boron doped NCD films have complex electronic behavior, a logarithmic relation between conductivity and temperature is observed at lower temperatures [29]. This can be related to a theoretical model for granular systems summarized by Beloborodov *et al* [47]. However, at higher temperatures the behavior cannot be described in a satisfactory manner by currently available theoretical models. In order to get a better idea about the electronic transport properties in B:NCD with different grain boundary densities, the set of samples discussed in the previous section was subjected to electronic transport measurements.

3.2.1. Resistivity. Firstly, one can see in figure 4 that the resistivity for samples investigated in this work decreases with decreasing C/H ratio. Secondly, $\partial\rho/\partial T$ is negative and also decreases with decreasing C/H ratio. The 1% sample, with the lowest resistivity and the lowest $|\partial\rho/\partial T|$, has resistivity properties closer to those of a heavily boron-doped single-crystal/microcrystalline

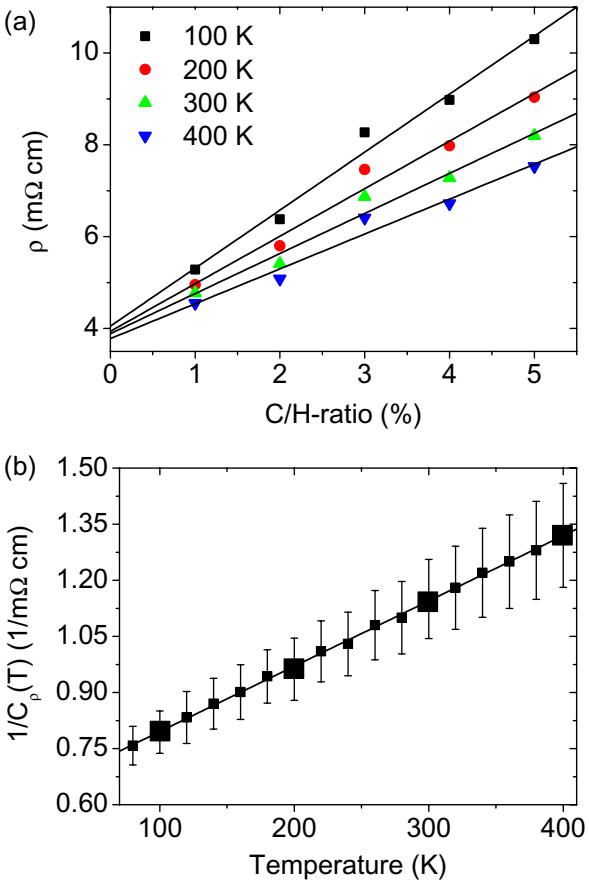

Figure 5. Panel (a) shows resistivity as a function of C/H ratio measured at different temperatures. For the sake of clarity, not all available data points obtained at other temperatures are plotted. The large data points on panel (b) are the inverse values of $C_\rho(T)$, plotted as a function of temperature. The small data points are the inverse values of $C_\rho(T)$, which are not shown on panel (a). This leads to the empirical expression $C_\rho(T) = 1/(A + BT)$.

diamond than the 5% sample [24, 43]. The 5% sample, with smaller grain size and thus more grain boundaries, shows the highest resistivity and the highest $|\partial\rho/\partial T|$, and thus shows resistivity properties closer to that of a grain boundary, as described above, than the 1% sample. When the degenerate grains themselves, with $\partial\rho/\partial T > 0$ [24, 43], have a lower resistivity than the grain boundaries, with $\partial\rho/\partial T < 0$, it can be concluded that a higher grain boundary density increases the resistivity and alters the temperature dependence of the resistivity.

Figure 5(a) shows linear fits of resistivity as a function of C/H ratio and, as is clear, the intercepts of those linear fits with the y-axis have almost the same value. Now, one can construct the following equation:

$$\rho = \rho_0 + \rho(\xi, T), \tag{4}$$

where ρ_0 represents the small temperature-dependent resistivity of a hypothetical sample grown at 0% C/H ratio, i.e. with the lowest degree of grain boundaries for a certain film thickness. In the light of the results discussed before, such a sample would correspond to a film with grains

of 150 nm. Only in the case of the hypothetical 'infinite' growth time would ρ_0 be equal to the resistivity of a heavily doped single crystal (ρ_{SC}). Hence, $\rho_0 > \rho_{SC}$. The temperature and the C/H ratio dependence are mainly represented by $\rho(\xi, T)$. For each temperature, the resistivity as a function of the C/H ratio is approximately linear (figure 5(a)). This means that $\rho(\xi, T)$ can be written as a function of the C/H ratio (ξ) with a temperature-dependent part $C_\rho(T)$:

$$\rho = \rho_0 + C_\rho(T)\xi. \tag{5}$$

From figure 5(a), one can deduce the values of ρ_0 and $C_\rho(T)$. Plotting the inverse of $C_\rho(T)$ as a function of temperature yields figure 5(b), where a remarkable linear relationship becomes visible. Hence, $1/C_\rho(T) \propto T$. Based on this, equation (5) can be written as

$$\rho = \rho_0 + \frac{\xi}{A + BT}. \tag{6}$$

Equation (6) is now used to fit the temperature dependence of the resistivity in figure 4 with ρ_0 as the only fitting parameter for the five different curves. A similar fit function was recently applied successfully to the temperature-dependent resistivity of ultra-thin graphite flakes [48]. The values of A and B are derived from the linear fit of figure 5(b), and the value of ρ_0, used for the initiation of the fitting parameter, is derived from the intercept of figure 5(a) ($\approx$3.9 mΩ cm). For low C/H ratios, the grain boundary density in the films is reduced and because $|\partial\rho/\partial T|$ is small and ρ_0 is very close to the value of a heavily boron-doped single-crystal/microcrystalline diamond ($\approx$2.8 mΩ cm) [24, 43], it can be approximated that ρ_0 is the resistivity contribution of a heavily boron-doped single-crystal diamond. In addition, this approximation becomes better by increasing the growth time of the films, leading to larger grains. The second resistivity contribution ($\rho(\xi, T)$) has a stronger temperature dependence and increases linearly with C/H ratio (figure 5(a)). The grain boundary density also increases with C/H ratio, and therefore this second resistivity contribution can be seen as the resistivity contribution of the grain boundaries (ρ_{GB}). Now, the total resistivity is the sum of two independent resistivity contributions, i.e. ρ_0 and $\rho(\xi, T)$. This proves that Matthiessen's rule is fulfilled, and equation (4) can now be written as

$$\rho = \rho_0 + \rho(\xi, T) = \rho_{SC} + \rho_{GB}. \tag{7}$$

In previous work, it was already observed that the temperature dependence of resistivity in B:NCD on the metallic side of the metal–insulator transition was positive instead of negative, although a negative dependence is expected for degenerate semiconductors. Therefore, an experimental activation energy (E_a) higher than 0 eV was obtained [25]. In order to derive an experimental activation energy, resistivity is fitted for an exponential dependence with $1/T$ (figure 6(a)). In the temperature region above 300 K, experimental activation energies are derived and summarized in table 2. Figure 6(b) shows that activation energy decreases as a function of C/H ratio and becomes very small for low C/H ratios, i.e. towards single-crystal/microcrystalline diamond on the metallic side of the metal–insulator transition [24, 43]. This is direct proof that a higher grain boundary density, related to a higher C/H ratio, increases E_a. The experimental activation energy seems to reach a maximum as a function of the C/H ratio and becomes very small at a theoretical C/H ratio of 0%. Therefore, a least squares fit with an exponential function

$$y = a - bx^c \tag{8}$$

Table 2. Summary of resistivity (ρ), hole mobility (μ) and hole density (n_{Hall}) derived from Hall effect measurements at 400 K. The experimental activation energy (E_{a}) of the 0.5% sample is derived by measuring its resistance and not its resistivity as for the other samples. The latter quantity is derived in the region of 300–400 K. The total boron concentration (n_{NDP}) is determined by NDP.

C/H ratio (%)	ρ (mΩ cm)	n_{Hall} (10^{21} cm^{-3})	n_{NDP} (10^{21} cm^{-3})	μ (cm^2 V^{-1} s^{-1})	E_{a} (meV)
0.5	–	–	–	–	4.0
1	4.6	1.8	3.3	0.77	5.4
2	5.1	2.1	3.1	0.59	7.3
3	6.4	2.3	3.4	0.43	8.0
4	6.7	2.7	4.0	0.34	9.2
5	7.5	2.8	5.3	0.30	9.6

is performed on the data set with $y = E_{\mathrm{a}}$ and $x = \xi$. The first of the three parameters ($a = 10.5 \pm 0.6$, $b = 8.0 \pm 0.4$, $c = 0.65 \pm 0.06$) can be used to estimate the maximum value of the experimental activation energy ($\approx$10.5 meV).

In order to explain the empirical equations, derived above, a theoretical model, proposed by Lu *et al* [49], is used. They proposed a modified trapping theory that turned out to be suitable for modeling the transport behavior in doped polycrystalline Si films. This model approximates resistivity as

$$\rho = \rho_{\mathrm{GB}} \left(\frac{2w}{d} \right) + \rho_{\mathrm{SC}} \left(1 - \frac{2w}{d} \right), \tag{9}$$

where ρ_{GB} is the resistivity induced by a grain boundary and caused by trapping of charge carriers in the grain boundary. The quantity w is the depletion width at each side of the grain boundary and d is the grain size. In equation (9), $2w/d$ represents the depleted fraction of the grain and $1 - (2w/d)$ represents the undepleted fraction. The equation also predicts that the resistivity of polycrystalline Si will approach, but not become lower than, that of single-crystal Si. When trapping is irrelevant or the grains are highly doped, $2w$ is the width of a grain boundary. Till now, no set of polycrystalline diamond samples could be related to this equation [25, 50]. Rewriting equation (9) results in

$$\rho = \rho_{\mathrm{SC}} + \frac{2w}{d} (\rho_{\mathrm{GB}} - \rho_{\mathrm{SC}}), \tag{10}$$

and by replacing $1/d$ with equation (3) one obtains

$$\rho = \rho_{\mathrm{SC}} + \left(A_d \xi + \frac{1}{d_0} \right) 2w \, (\rho_{\mathrm{GB}} - \rho_{\mathrm{SC}}). \tag{11}$$

Comparing the latter equation with equation (5) gives

$$\rho_0 = \rho_{\mathrm{SC}} + \frac{2w \, (\rho_{\mathrm{GB}} - \rho_{\mathrm{SC}})}{d_0} \tag{12}$$

and

$$C_\rho(T) = A_d 2w \, (\rho_{\mathrm{GB}} - \rho_{\mathrm{SC}}). \tag{13}$$

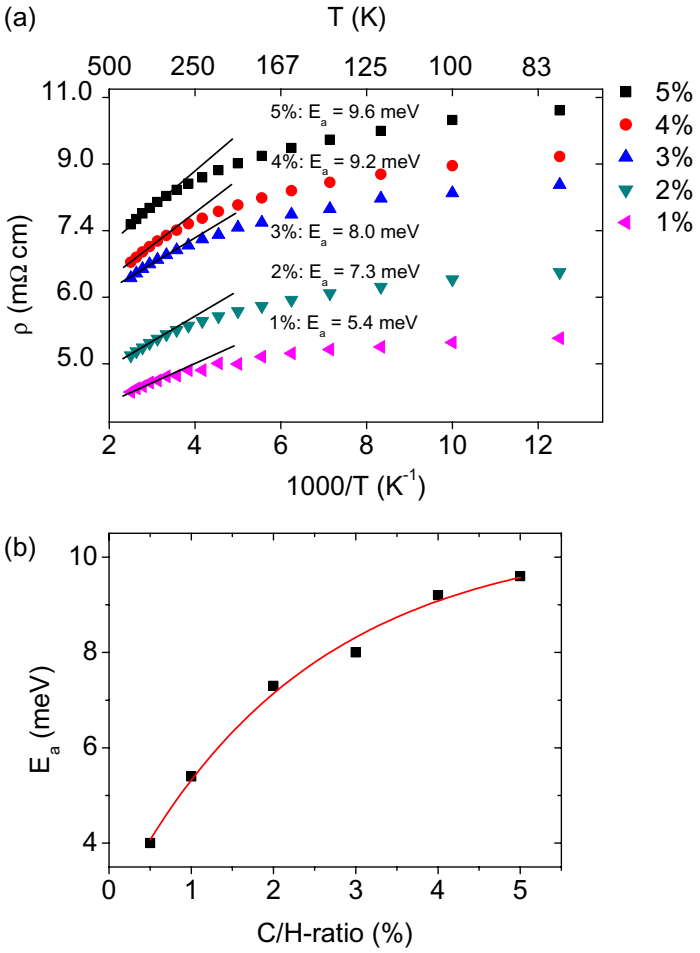

Figure 6. Panel (a) shows resistivity, fitted for exponential dependence with $1/T$. From 300 to 400 K, experimental activation energies are derived. In panel (b), activation energy as a function of C/H ratio is fitted (least squares) with equation (8). One can conclude that E_a decreases as a function of grain size.

As explained before, the quantity $1/d_0$ becomes $0\,\mathrm{nm}^{-1}$ for infinite growth times, i.e. the grain boundary density approaches zero and makes $\rho_0 = \rho_{SC}$. This supports the earlier assumption that $\rho_0 \approx \rho_{SC}$. In support, a boron-doped microcrystalline diamond with the same active charge carrier concentration as the 1% sample has a resistivity of 2.8 mΩ cm [43], which is lower than the value at a C/H ratio of 0% (≈3.9 mΩ cm). This is expected since ρ_0 is not yet equal to ρ_{SC} due to the finite growth times used in this work.

A complete procedure for deriving w and ρ_{GB} with low charge carrier concentrations and with thermionic emission as the dominant temperature-dependent transport process is explained in the work of Lu *et al* [49]. Due to the high doping levels in samples of this work, exact electronic transport processes are difficult to derive, which makes the determination of the values of w and ρ_{GB} impossible in practice. When performing a linear fit with w and ρ_{GB} as the only fitting parameters, the fit will not converge, which means that multiple solutions for the values of w and ρ_{GB} are possible. When the average grain boundary thickness is measured by e.g. transmission electron microscopy and one assumes that $2w$ is the width of the grain

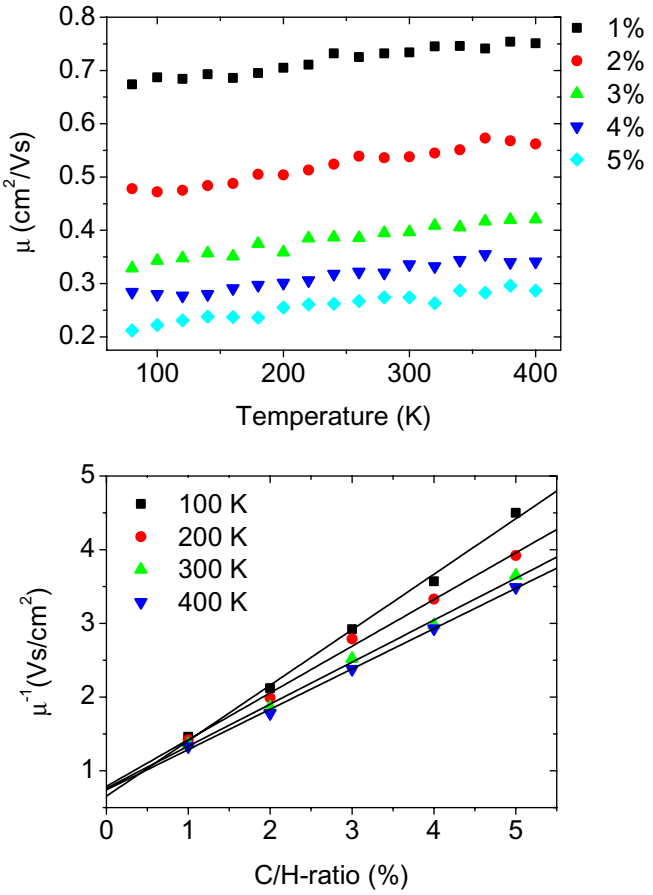

Figure 7. Panel (a) shows mobility as a function of temperature for different C/H ratios. All samples show a small increase in mobility as a function of temperature. Panel (b) shows inverse mobility values as a function of C/H ratio measured at different temperatures.

boundary, ρ_{GB} can be calculated. At the end of this section, after handling the charge carrier mobility/density, a more detailed treatment of the temperature-dependent transport properties is given.

3.2.2. Mobility. Due to scattering at boron impurities, the hole mobility in a heavily boron-doped single-crystal diamond is strongly reduced when compared to a low boron-doped single-crystal diamond [24, 51]. Grain boundaries also reduce the mobility by scattering and this is clear in figure 7(a), where the mobility in the layers is strongly reduced as a function of C/H ratio. The mobility values in the investigated films are calculated with the assumption that no n-type carriers are present [52]. Figure 7(a) also shows that the change in charge carrier mobility as a function of temperature ($\partial\mu/\partial T$) is slightly positive. Therefore, the hole mobility in all samples is thermally activated, as expected when a number of grain boundaries is present. When comparing the mobility values of the 1 and 5% samples, two observations can be made. Firstly, the mobility of the former is comparable to that of a highly boron-doped single-crystal diamond [24] ($\approx 4\,\mathrm{cm^2\,V^{-1}\,s^{-1}}$) and microcrystalline diamond layer ($\approx 1.7\,\mathrm{cm^2\,V^{-1}\,s^{-1}}$), but

lower due to the contributions of grain boundaries. Secondly, as grain boundaries are more present, mobility shows a decrease with increasing C/H ratio. For all temperatures, the inverse of the mobility is linear as a function of C/H ratio (figure 7(b)) so the mobility can be expressed as

$$\frac{1}{\mu} = \frac{1}{\mu_0} + C_\mu(T)\xi, \tag{14}$$

where $1/\mu_0$ is approximated as a quasi-constant intercept in figure 7(b). Since μ_0 approaches the value of boron-doped single-crystal diamond [24], it can be interpreted as the hole mobility in heavily boron-doped single-crystal diamond (μ_{SC}). The quantity $C_\mu(T)\xi$ is mainly the contribution of the grain boundaries to the hole mobility since the grain boundary density increases as a function of C/H ratio. Again, Matthiessen's rule is fulfilled since the inverse of the mobility contribution of the grain boundaries is added to the inverse of the mobility in the heavily doped diamond grains, giving the total inverse mobility presented in the following equation:

$$\frac{1}{\mu} = \frac{1}{\mu_{SC}} + \frac{1}{\mu_{GB}}. \tag{15}$$

Again, using the theory of Lu *et al* [49] mobility is written as follows:

$$\frac{1}{\mu} = \frac{1}{\mu_{GB}}\left(\frac{2w}{d}\right) + \frac{1}{\mu_{SC}}\left(1 - \frac{2w}{d}\right), \tag{16}$$

where μ_{GB} is the mobility induced by a grain boundary. Rewriting equation (16) results in

$$\frac{1}{\mu} = \frac{1}{\mu_{SC}} + \frac{2w}{d}\left(\frac{1}{\mu_{GB}} - \frac{1}{\mu_{SC}}\right), \tag{17}$$

and by replacing $1/d$ with equation (3) one obtains

$$\frac{1}{\mu} = \frac{1}{\mu_{SC}} + \left(A_d\xi + \frac{1}{d_0}\right)2w\left(\frac{1}{\mu_{GB}} - \frac{1}{\mu_{SC}}\right). \tag{18}$$

Comparing the latter equation with equation (14) gives

$$\frac{1}{\mu_0} = \frac{1}{\mu_{SC}} + \frac{2w}{d_0}\left(\frac{1}{\mu_{GB}} - \frac{1}{\mu_{SC}}\right) \tag{19}$$

and

$$C(T) = A_d 2w\left(\frac{1}{\mu_{GB}} - \frac{1}{\mu_{SC}}\right). \tag{20}$$

Again, the quantity $1/d_0$ becomes $0\,\mathrm{nm}^{-1}$ for infinite growth times, which makes $\mu_0 = \mu_{SC}$. This supports the earlier made approximation that $\mu_0 \approx \mu_{SC}$. The boron-doped microcrystalline diamond with the same active charge carrier concentration as the 1% sample has a hole mobility of $1.7\,\mathrm{cm}^2\,\mathrm{V}^{-1}\,\mathrm{s}^{-1}$ [43], which is higher than μ_0 ($1.3\,\mathrm{cm}^2\,\mathrm{V}^{-1}\,\mathrm{s}^{-1}$). This is expected since μ_0 is not yet equal to μ_{SC} and to the mobility of a heavily doped microcrystalline diamond due to the finite growth times used in this work.

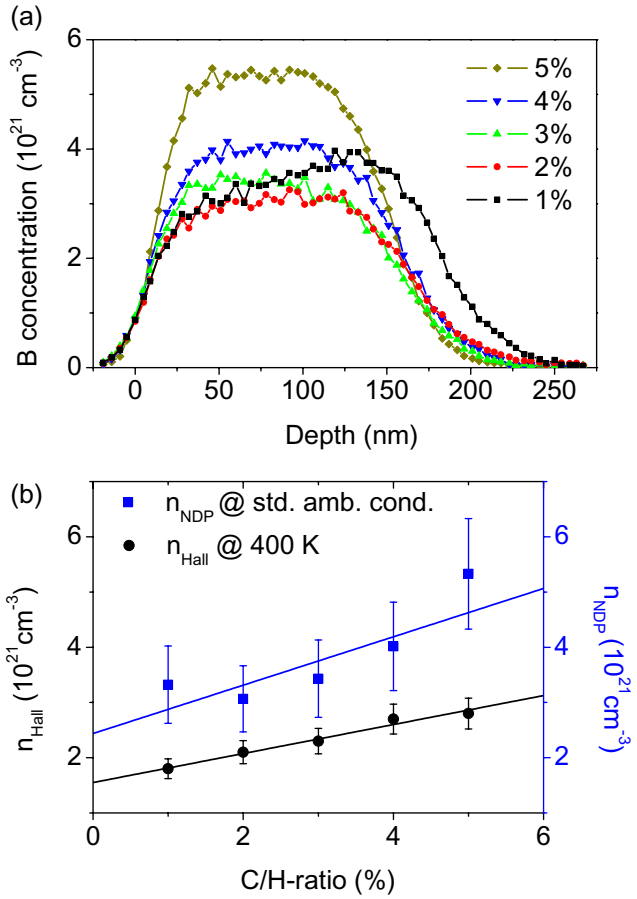

Figure 8. Panel (a) shows the NDP spectrum of boron for NCD layers, measured at standard ambient conditions. Panel (b) shows the total boron concentration (n_{NDP}) and the hole concentration (n_{Hall}), measured at 400 K, as a function of C/H ratio. These values are listed in table 2.

3.2.3. Charge carriers. Active charge carrier concentrations for B:NCD films (n_{Hall}) greater than 10^{21} cm^{-3} are derived from Hall effect measurements, and total boron concentrations (n_{NDP}) are derived from NDP (figure 8(a)). Charge carrier concentrations, determined at 400 K, show a linear relation with C/H ratio, and boron concentrations, calculated from NDP, show an increase as a function of C/H ratio (figure 8(b)). For all samples, n_{Hall} increases slightly with temperature (figure 9(a)). The active boron concentration (n_{Hall}/n_{NDP}) at 400 K is estimated to be about 50–70%. For higher C/H ratios, more boron is incorporated actively into the diamond lattice, which was earlier observed in single-crystal diamond [31].

However, the inactive incorporation of boron also increases, even more than the inactive incorporation, and therefore, the active boron concentration decreases as a function of C/H ratio. This could indicate that inactive boron is located in the grain boundaries as they are more plentiful at higher C/H ratios. Resistivity as a function of C/H ratio is not highly related to charge carrier density since charge carrier density should decrease as a function of C/H ratio to make resistivity increase as a function of C/H ratio, an effect that is present even if the amount of incorporated boron is higher. The decrease in mobility as a function of C/H ratio is thus

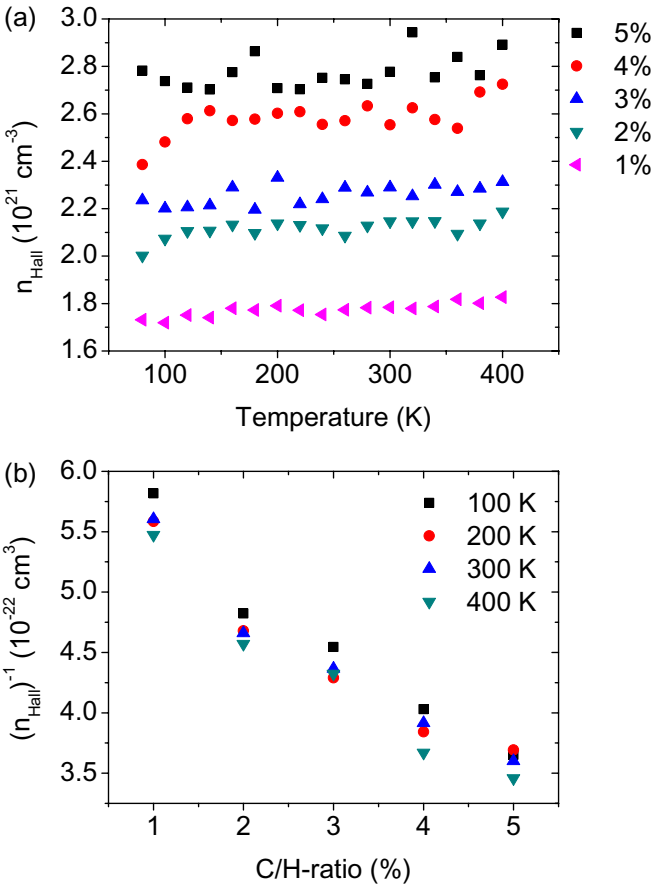

Figure 9. Panel (a) shows the charge carrier density (n_{Hall}) derived from Hall effect measurements as a function of temperature for different C/H ratios. The charge carrier density increases slightly as a function of temperature. Panel (b) shows the inverse n_{Hall} values as a function of the C/H ratio measured at different temperatures.

mainly responsible for the increase in resistivity as a function of C/H ratio. At different growth conditions, 'cauliflower'-type nanocrystalline (c-NCD) and ultrananocrystalline CVD diamond films can be generated, and the affinity of boron to the surface of the grains and to the grain boundaries becomes more important [53, 54]. Since the morphology of the latter films differs from the morphology of the films in this work, transport mechanisms other than those suggested in this work most probably occur there.

3.2.4. Temperature dependence. To explain the increase in $|\partial\rho/\partial T|$ as a function of C/H ratio, one has to look at the temperature dependence of one over the charge carrier density/mobility as a function of C/H ratio since $\rho \propto 1/(\mu n_{\mathrm{Hall}})$. From figure 7(b) it is easily derived that $|\partial\mu^{-1}/\partial T|$ increases as a function of C/H ratio, which explains the increase in $|\partial\rho/\partial T|$ as a function of C/H ratio. When making the same exercise for n_{Hall}, no significant change of $|\partial n_{\mathrm{Hall}}^{-1}/\partial T|$ as a function of C/H ratio can be seen (figure 9(b)). The slow increase of charge carrier density/mobility as a function of temperature is very difficult to explain. Qualitatively, it

is possible to address the mobility increase as a function of temperature to ionized impurity scattering ($\mu \propto T^{3/2}$) [46], impurity-band conduction [55], tunneling conductance between grains [47, 56] and thermionic emission [49]. The temperature dependence of resistivity, related to thermally activated mobility, is an indication that grain boundaries alter the temperature dependence of electronic transport properties. The charge carrier density increase as a function of temperature can be addressed with respect to acceptor ionization, although one has to keep in mind that the samples in this work are on the metallic side of the metal–insulator transition. The drawback is that temperature-dependent effects, rising from grain boundaries, are masked, which is explained by Lu *et al* [49]. They state that the grain barriers in polycrystalline films decrease in width as a function of charge carrier concentration, which results in resistivity containing barrier and bulk components that affect its temperature behavior. To investigate this in more detail, low levels of doping would be required. However, this would in turn increase the resistivity of such films, complicating measurements by, among other things, inducing lower signal-to-noise levels.

4. Conclusions

The results in this work confirm that a low C/H ratio during the growth of heavily boron doped NCD on the metallic side of the metal–insulator transition leads to larger grains and a higher surface roughness than for a high C/H ratio. Electronic transport measurements reveal a lower resistivity, a higher hole mobility and a lower carrier density for lower C/H ratios. The difference in resistivity as a function of temperature is less pronounced for lower C/H ratios, which is strongly related to mobility. Since the grain boundary density is higher for films grown with high C/H ratios, their electronic transport properties resemble more the electronic transport properties of grain boundaries, although a clear origin of the temperature dependence is still lacking. Contributions for the resistivity and mobility of grain boundaries and grains can be independently identified. Hereby, Matthiessen's rule and a theory that describes the transport properties in polycrystalline silicon are followed. It is also shown that the boron incorporation for B:NCD and the active/inactive charge carrier concentration increase significantly when the B/C ratio is kept constant and the C/H ratio is increased.

Acknowledgments

This work was financially supported by the Research Foundation-Flanders (FWO) (Projects G.0430.07 & G.0555.10N), the Belgian Science Policy (BELSPO) (IAP-P6/42), the Methusalem network 'NANO' Antwerp-Hasselt, the EC (FP7 projects MATCON & MOLESOL, MATERA+ project ACIN) and the Academy of Sciences of the Czech Republic (Research Project no. KAN400480701 and MSM6840770012).

References

[1] Kriele A, Williams O A, Wolfer M, Brink D, Muller-Sebert W and Nebel C E 2009 *Appl. Phys. Lett.* **95** 031905
[2] Bi B, Huang W, Asmussen J and Golding B 2002 *Diam. Relat. Mater.* **11** 677
[3] Benedic F, Assouar M B, Mohasseb F, Elmazria O, Alnot P and Gicquel A 2004 *Diam. Relat. Mater.* **13** 347
[4] Dipalo M, Kusterer J, Janischowsky K and Kohn E 2006 *Phys. Status Solidi* A **203** 3036

[5] Kubovic M, Janischowsky K and Kohn E 2005 *Diam. Relat. Mater.* **14** 514
[6] Lim C H Y X L, Zhong Y L, Janssens S D, Nesladek M and Loh K P 2010 *Adv. Funct. Mater.* **20** 1313
[7] Hartl A, Schmich E, Garrido J A, Hernando J, Catharino S C R, Walter S, Feulner P, Kromka A, Steinmuller D and Stutzmann M 2004 *Nat. Mater.* **3** 736
[8] Siew P S, Loh K P, Poh W C and Zhang H 2005 *Diam. Relat. Mater.* **14** 426
[9] Wenmackers S *et al* 2008 *Langmuir* **24** 7269
[10] Abouzar M H, Poghossian A, Razavi A, Besmehn A, Bijnens N, Williams O A, Haenen K, Wagner P and Schoning M J 2008 *Phys. Status Solidi* A **205** 2141
[11] McCauley T G, Gruen D M and Krauss A R 1998 *Appl. Phys. Lett.* **73** 1646
[12] Lee J, Hong B, Messier R and Collins R 1996 *Appl. Phys. Lett.* **69** 1716
[13] Hong B Y, Lee J, Collins R W, Kuang Y L, Drawl W, Messier R, Tsong T T and Strausser Y E 1997 *Diam. Relat. Mater.* **6** 55
[14] Williams O A and Nesladek M 2006 *Phys. Status Solidi* A **203** 3375
[15] Daenen M, Williams O A, D'Haen J, Haenen K and Nesladek M 2006 *Phys. Status Solidi* A **203** 3005
[16] Williams O A, Kriele A, Hees J, Wolfer M, Muller-Sebert W and Nebel C E 2010 *Chem. Phys. Lett.* **495** 84
[17] Chen Q Y, Gruen D M, Krauss A R, Corrigan T D, Witek M and Swain G M 2001 *J. Electrochem. Soc.* **148** E44
[18] May P W, Ashfold M N R and Mankelevich Y A 2007 *J. Appl. Phys.* **101** 053115
[19] Achatz P *et al* 2009 *Phys. Status Solidi* A **206** 1978
[20] Willems B L, Zhang G, Vanacken J, Moshchalkov V V, Janssens S D, Williams O A, Haenen K and Wagner P 2009 *J. Appl. Phys.* **106** 033711
[21] Bachmann P K, Leers D and Lydtin H 1991 *Diam. Relat. Mater.* **1** 1
[22] Butler J E and Woodin R L 1993 *Phil. Trans. R. Soc.* A **342** 209
[23] Wild C, Kohl R, Herres N, Muller-Sebert W and Koidl P 1994 *Diam. Relat. Mater.* **3** 373
[24] Borst T H and Weis O 1995 *Diam. Relat. Mater.* **4** 948
[25] Gajewski W, Achatz P, Williams O A, Haenen K, Bustarret E, Stutzmann M and Garrido J 2009 *Phys. Rev.* B **79** 045206
[26] Ekimov E A, Sidorov V A, Bauer E D, Mel'nik N N, Curro N J, Thompson J D and Stishov S M 2004 *Nature* **428** 542
[27] Nesladek M, Mares J J, Tromson D, Mer C, Bergonzo P, Hubik P and Kristofik J 2006 *Sci. Technol. Adv. Mater.* **7** 41
[28] Mares J J, Hubik P, Kristofik J and Nesladek M 2008 *Sci. Technol. Adv. Mater.* **9** 044101
[29] Achatz P *et al* 2009 *Phys. Rev.* B **79** 201203
[30] Zhang G, Vanacken J, Van de Vondel J, Decelle W, Fritzsche J, Moshchalkov V V, Willems B L, Janssens S D, Haenen K and Wagner P 2010 *J. Appl. Phys.* **108** 013904
[31] Bustarret E 2008 *Phys. Status Solidi* A **205** 997
[32] Williams O A, Douheret O, Daenen M, Haenen K, Osawa E and Takahashi M 2007 *Chem. Phys. Lett.* **445** 255
[33] Mortet V, Nesladek M, Haenen K, Morel A, D'Olieslaeger M and Vanecek M 2004 *Diam. Relat. Mater.* **13** 1120
[34] Hnatowicz V, Vacik J and Fink D 2010 *Rev. Sci. Instrum.* **81** 073906
[35] Kromka A, Grausova L, Bacakova L, Vacik J, Rezek B, Vanecek M, Williams O A and Haenen K 2010 *Diam. Relat. Mater.* **19** 190
[36] Vacik J, Hnatowicz V, Cervena J, Posta S, Koster U and Pasold G 2009 *AIP Conf. Proc.* **1099** 836
[37] Jiang H G, Ruhle M and Lavernia E J 1999 *J. Mater. Res.* **14** 549
[38] Wild C, Koidl P, Muller-Sebert W, Walcher H, Kohl R, Herres N, Locher R, Samlenski R and Brenn R 1993 *Diam. Relat. Mater.* **2** 158
[39] Cullity B D and Stock S R 1956 *Elements of X-ray Diffraction* (Reading, MA: Addison-Wesley)
[40] Wertheim G K 1974 *Rev. Sci. Instrum.* **45** 1369

[41] Sanchez-Bajo F, Ortiz A L and Cumbrera F L 2006 *Acta Mater.* **54** 1
[42] Willems B L *et al* 2009 *Phys. Rev.* B **80** 224518
[43] Werner M *et al* 1994 *Appl. Phys. Lett.* **64** 595
[44] Klein T *et al* 2007 *Phys. Rev.* B **75** 165313
[45] Nebel C E 2003 *Semicond. Sci. Technol.* **18** S1
[46] Lundstrom M 2000 *Fundamentals of Carrier Transport* 2nd edn (Cambridge: Cambridge University Press)
[47] Beloborodov I S, Lopatin A V, Vinokur V M and Efetov K B 2007 *Rev. Mod. Phys.* **79** 469
[48] Vansweevelt R, Mortet V, D'Haen J, Ruttens B, Van Haesendonck C, Partoens B, Peeters F M and Wagner P 2011 *Phys. Status Solidi* A **208** 1252
[49] Lu N C, Gerzberg L, Lu C and Meindl J D 1981 *IEEE Trans. Electron Devices* **28** 818
[50] Malta D M, von Windheim J A, Wynands H A and Fox B A 1996 *J. Appl. Phys.* **77** 1536
[51] Pernot J, Volpe P N, Omnes F, Muret P, Mortet V, Haenen K and Teraji T 2010 *Phys. Rev.* B **81** 205203
[52] Smith R A 1959 *Semiconductors* (Cambridge: Cambridge University Press)
[53] May P W, Ludlow W J, Hannaway M, Heard P J, Smith J A and Rosser K N 2008 *Diam. Relat. Mater.* **17** 105
[54] Barnard A S and Sternberg M 2006 *J. Phys. Chem.* B **110** 19307
[55] Fritzsche H and Cuevas M 1960 *Phys. Rev.* **119** 1238
[56] Sheng P 1980 *Phys. Rev.* B **21** 2180